International Journal of Applied Electromagnetics and Mechanics 42 (2013) 119–136
DOI 10.3233/JAE-131650
IOS Press

Magnetic field due to a finite current carrying disk considering a variable current density along its radial dimension

Guillermo A. Díaz Flórez* and Enrique Esteban Mombello
Instituto de Energía Eléctrica, Universidad Nacional de San Juan, San Juan, Argentina

Abstract. This paper proposes a fast and accurate methodology to calculate the magnetic field produced by a finite disk considering a linear variation of the current density between the inner and the outer radius. The mathematical expressions have been developed with the aim of reducing the computational effort, while ensuring accurate and reliable results. Additionally, the strategies presented in this work provide expressions which are free of singularities.

Keywords: Finite disk, Biot-Savart law, quadrature, magnetic field

1. Introduction

In the field of magnetic modeling of electrical equipment, it is very important to determine the magnetic field produced by current carrying elements with disk shaped geometry. One clear example of this is a power transformer winding, which is usually manufactured using disk or helical coils with radial conductors in parallel [1]. These coils can be satisfactorily represented by an array of disks having infinitesimal thickness. In the case of axisymmetric geometry, the magnetic field produced by disk-shaped elements having a linear variation of the current density can be used to represent the magnetization current in the transformer yokes.

The semi-analytical expressions for the magnetic field of a disk carrying a constant current density have been previously presented in the literature by Babic et al. [3]. However, as far as the authors of this article know, expressions considering the linear variation of current density have not been introduced yet. It is important to highlight that this work is a generalization of the method proposed by Babic et al. [3] in the sense of considering now a variable current density. Analytical expressions for the magnetic vector potential are also presented (which had not been presented in [3]).

1.1. Statement of the problem

This work pursues to propose a computationally efficient method to determine the vector potential A_ϕ and the magnetic field strength in both radial H_r and axial H_z directions produced by a finite disk, so that the calculations are fast enough and a reasonable accuracy for engineering applications can be achieved.

*Corresponding author: Guillermo A. Díaz Flórez, Instituto de Energía Eléctrica (IEE), Universidad Nacional de San Juan (UNSJ), Av. Libertador San Martín 1109 (Oeste), San Juan, P.C. J5400ARL, Argentina. Tel.: +54 264 422 6444; E-mail: guillermoandresdiaz@gmail.com.

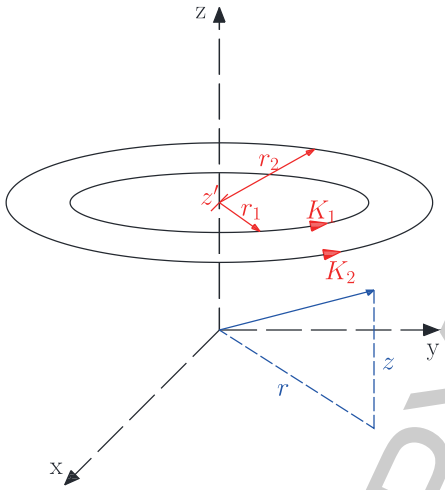

Fig. 1. Current carrying disk geometry.

2. Basic expressions

This section presents the mathematical expressions for the magnetic field due to a finite disk with inner radius r_1 (m), where the sheet current density is K_1 (A/m), and outer radius r_2 (m), where the sheet current density is K_2 (A/m). The axis of the disk is considered to be on the z axis at a distance z' (m) from the x-y plane. The magnetic field produced by the disk is calculated at a general observation point P (r, z). Figure 1 shows the disk geometry.

2.1. Magnetic vector potential

By application of the Biot-Savart law, the magnetic vector potential at point P (r, z) produced by a filamentary circular loop which carries a current I_ϕ and with radius r' is given by the following expression [7]

$$A_\phi^{[st]} = \frac{\mu_0 I_\phi}{2\pi} \int_0^\pi \frac{\cos(\phi')r'}{\sqrt{r^2 + r'^2 + (z - z')^2 - 2rr'\cos(\phi')}} \mathrm{d}\phi' \tag{1}$$

where the primed coordinates are related with the source of field, and the not primed coordinates with the observation point, also called field point. On the assumption that the sheet current density K_ϕ varies linearly between the inner radius r_1 and the outer radius r_2 according to Eq. (2), the current carried by an infinitesimal disk having a radial width $\mathrm{d}r'$ is $I_\phi = K_\phi(r')\mathrm{d}r'$.

$$K_\phi(r') = K_2 \frac{r' - r_1}{r_2 - r_1} - K_1 \frac{r' - r_2}{r_2 - r_1} \tag{2}$$

Considering the differential contribution of current I_ϕ, integrating between r_1 and r_2 the expression of the magnetic vector potential due to a current carrying disk with a linear variation of the current density is obtained,

$$A_\phi{}^{[fd]} = \frac{\mu_0}{2\pi} \int_{r_1}^{r_2} \int_0^\pi \frac{K_\phi(r')\cos(\phi')r'}{\sqrt{r^2 + r'^2 + (z - z')^2 - 2rr'\cos(\phi')}} \mathrm{d}\phi' \mathrm{d}r' \tag{3}$$

For the sake of simplicity, the sheet current density $K_\phi(r')$ is called K in the following. The function in the integral in Eq. (3) can be named as

$$f_A\left(\phi', r'\right) = \frac{K\cos\left(\phi'\right) r'}{\sqrt{r^2 + r'^2 + \left(z - z'\right)^2 - 2rr'\cos\left(\phi'\right)}} \tag{4}$$

which will be used in the following equations. Additionally, calling $A_\phi{}^{[fd]}$ just A_ϕ, the magnetic vector potential can be expressed as

$$A_\phi = \frac{\mu_0}{2\pi}\int_0^\pi \int_{r_1}^{r_2} f_A\left(\phi', r'\right) \mathrm{d}r'\mathrm{d}\phi' \tag{5}$$

Although f_A is not only a function of the variables ϕ' and r', they are the only variables to be considered as integration variables in Eq. (5).

2.2. Magnetic field intensity in the radial direction

The magnetic flux density $\vec{\boldsymbol{B}}$ is related to the magnetic vector potential by

$$\vec{\boldsymbol{B}} = \hat{\boldsymbol{r}}B_r + \hat{\boldsymbol{\phi}}B_\phi + \hat{\boldsymbol{z}}B_z = \nabla \times \vec{\boldsymbol{A}} \tag{6}$$

Since this problem is formulated in cylindrical coordinates, and the magnetic vector potential has only a ϕ component ($\vec{\boldsymbol{A}} = \hat{\boldsymbol{\phi}}A_\phi$), it follows from Eq. (6) that the magnetic flux density in the radial direction B_r is given by

$$B_r = -\frac{\partial A_\phi}{\partial z} \tag{7}$$

Assuming that the cylinder is located in a homogeneous medium with magnetic permeability equal to the vacuum, the following constitutive relation holds

$$\vec{\boldsymbol{B}} = \mu_0\vec{\boldsymbol{H}} = \mu_0\left(\hat{\boldsymbol{r}}H_r + \hat{\boldsymbol{\phi}}H_\phi + \hat{\boldsymbol{z}}H_z\right) \tag{8}$$

Thus, replacing Eq. (7) in Eq. (8) and solving for H_r, the following expression is obtained

$$H_r = -\frac{1}{\mu_0}\frac{\partial A_\phi}{\partial z} \tag{9}$$

Substituting Eq. (5) in Eq. (9) and rearranging, the magnetic field strength in the radial direction is obtained

$$H_r = -\frac{1}{2\pi}\int_0^\pi \int_{r_1}^{r_2} \frac{\partial}{\partial z} f_A\left(\phi', r'\right) \mathrm{d}r'\mathrm{d}\phi' \tag{10}$$

2.3. Magnetic field intensity in the axial direction

In this case, it follows from Eq. (6) that the magnetic flux density in the axial direction B_z is given by

$$B_z = \frac{1}{r}\frac{\partial\left(rA_\phi\right)}{\partial r} \tag{11}$$

hence

$$H_z = \frac{1}{\mu_0 r}\frac{\partial\left(rA_\phi\right)}{\partial r} \tag{12}$$

The substitution of Eq. (5) in Eq. (12) leads to the expression of the magnetic field intensity in the axial direction

$$H_z = \frac{1}{2\pi r}\int_0^{\pi}\int_{r_1}^{r_2}\frac{\partial}{\partial r}\left(r f_A\left(\phi', r'\right)\right)\mathrm{d}r'\mathrm{d}\phi' \tag{13}$$

Finally, notice that from $\nabla \times \hat{\boldsymbol{\phi}} A_\phi$ in Eq. (6) it follows that $B_\phi = 0$, and therefore $H_\phi = 0$.

3. Integration by quadrature

As it will be shown in Section 4, the use of numerical integration to solve the integrals associated with the field produced by the disk is inevitable; therefore this section gives a brief introduction to the integration by quadratures, which will be of great importance for the development of this work. Suppose that the integral of a function $g(y)$ in the interval $[a, b]$ will be numerically solved. It can be shown that by the definition of a new variable $y = cx + d$ where $c = \frac{b-a}{2}$ and $d = \frac{b+a}{2}$ it is possible to transform the original integral into an equivalent one, now evaluated in the interval $[-1, 1]$ as follows,

$$S_a^b\left(g\right) = \int_a^b g(y)\mathrm{d}y = c\int_{-1}^{1} f(x)\mathrm{d}x \tag{14}$$

This transformation is important, since the quadratures in the literature are normally referred to a normalized integration range $[-1, 1]$, so that the numerical integration of the function $f(x)$ can be approximated by quadrature as follows

$$S_{-1}^1\left(f\right) = \int_{-1}^{1} f(x)\mathrm{d}x = \sum_{i=1}^{n_q} w_i f\left(x_i\right) + E_n \tag{15}$$

where w_i are the weights and x_i the quadrature nodes. The latter ones are usually zeros of certain orthogonal polynomials. Additionally, there is an error term E_n, which represents the error in the approximation of the integral using n_q nodes.

In the framework of this article, it is convenient to classify the methods of numerical integration in two categories, one associated with the selection of the node coordinates, and the other according to the error control mechanism, as presented below.

1. According to the selection of the node coordinates
   a. *Closed type*: The coordinates of the nodes include the limits of integration.
   b. *Open type*: Nodes never coincide with the limits of integration.

2. According to the error control mechanism
   a. *Adaptive*: In this type of scheme, the integral is strategically divided into subregions, such that the number of nodes used is increased in the subregions where the integrand presents important variations. This process is usually done recursively, and in each iteration it is verified that the error is less than a certain predefined value. When the error limit is satisfied, the process ends and the integral value is reported.
   b. *Direct*: In this paper, the method based on a fixed predefined number of nodes and weights is called direct integration. The main advantage of this method is that the integral is obtained in one step. In contrast to the adaptive method, the error in this methodology can not be controlled while the integral is calculated. This is why usually a generous amount of nodes is used in order to ensure a reasonable accuracy of the integral. The main advantage of the direct method is its high speed compared with adaptive methods. Normally, the determination of the weights w_i involves a large calculation overload, however, if the number of nodes is predefined, it is possible to determine the weights off-line and keep them ready to be used in any moment.

4. Strategies for solving the disk field integrals

Considering Eqs (5), (10) and (13), the ideal situation would be to find a fully analytical solution for the double integral which can be evaluated in one step. Unfortunately, several researchers have shown that the field equations produced by disk-shaped elements *do not have a fully closed analytical solution*. In fact, it has been shown that neither it is possible to fully express them as elliptic integral functions [2–6]. Unfortunately, the Eqs (5), (10) and (13) are no exception to the rule just mentioned, since they include expressions of the form

$$\int_0^{\pi} \cos\left(\phi'\right) \ln\left(r' - r\cos\left(\phi'\right) + \sqrt{r^2 + r'^2 + \left(z - z'\right)^2 - 2rr'\cos\left(\phi'\right)}\right) \mathrm{d}\phi' \tag{16}$$

which, as discussed in [2], does not belong to the set of elliptic integrals and must be evaluated numerically. Among the different strategies for the numerical solution of the field equations of the disk, the following ones can be mentioned:

1. *Fully numerical solution*: This strategy solves the integrals in a fully numerical way, using adaptive schemes of double quadrature. The main disadvantage of this strategy is that the nodes and weights are calculated adaptively for each integral (assuming that there are more than one source or more than one evaluation point), and their reuse is not possible. On the other hand, for some quadrature rules the determination of the weights can be a computationally expensive task increasing dramatically the calculation times [8].
2. *Semi-analytic solution*: In this strategy the integrals are solved analytically as far as possible using transformations to elliptic integrals and other special functions. The expressions that can not be reduced to the mentioned functions are evaluated numerically by means quadrature. This is the strategy that has been historically followed by several authors to solve the field expressions of different geometric configurations [2–6].
3. *1D analytical – 1D numerical solution*: It can be shown that the integrands of Eqs (5), (10) and (13) can be analytically integrated with respect to any of the variables of integration. The integration of $f_A\left(\phi', r'\right)$ with respect to ϕ' or with respect to r' lead to fully elliptical or fully analytical expressions respectively. This suggests the application of a mixed strategy in which the integral is analytically solved with respect to one variable and numerically with respect to the other one.

5. Selection of the strategy, method and quadrature rule

5.1. Strategy selection

In this specific case it is assumed that the values of both the vector potential and the magnetic field in radial and axial directions produced by a significant amount of field sources (disks) are needed at a large number of evaluation points. Additionally, although the calculation speed is considered critical, a reasonable accuracy is also needed. As it has been mentioned, there are three different strategies for solving the field equations of the disk numerically. The first strategy based on double numerical integration is disregarded because the calculation time is prohibitive for applications involving a large amount of field sources and evaluation points.

Although the second strategy, called semi-analytic, improves the computational performance compared with the first strategy, it is computationally intensive because the elliptic integrals must also be evaluated numerically [10]. It is shown in [11] that in a fully analytical method, the solution of the elliptic integrals can be effectively reused in further calculations. Although in a direct quadrature method the nodes and weights are reused in further integrals, in a semi-analytic strategy this advantage get partially lost. Another drawback of the semi-analytic solution is that the singularities of the elliptic integrals or the singularities in the integrands of non-elliptical expressions must be treated separately.

Consequently, the *1D analytical – 1D numerical* method is proposed for the computations, so that the first integrals of $f_A(\phi', r')$ are solved analytically with respect to r' as a first step, and then the integrals with respect to ϕ' are solved numerically. Additionally, a direct scheme has been used for the numerical integration, which has been tuned by means of a careful analysis of the error. The number of nodes was predefined ensuring fast and reliable results even under singularity conditions.

5.2. Selection of quadrature rule

As shown in Section 7, the integrands of the integrals to be solved have singularities precisely on one of the limits of integration, so that closed integration rules are not an option. Furthermore, it is evident that the integrands have a strong variation near the singularity, therefore a quadrature rule that concentrates more nodes near to the singularity is needed in order to correctly consider the variation of the function. Consequently, integration rules using equidistant distribution of nodes are not a good choice in this case.

Clearly, the selection of the optimal quadrature that correctly approximates the integral of a function in all possible cases (including singularities) ensuring short calculation times is not a trivial issue. After an analysis of possible integration methods, the Gauss-Legendre rule has shown as a very accurate and fast method, fulfilling the two conditions required for this specific application. In fact, Gauss-Legendre quadrature rule is one of the most widely used methods in computational routines of specialized programs because it has the highest possible degree of precision [8]. Theoretically, this quadrature rule provides exact results using n_q nodes in polynomials of degree up to $2n_q - 1$, which can be proved by direct derivation from the error term of Gauss-Legendre quadrature.

$$E_n = \frac{2^{2n_q+1}\left(n_q!\right)^4}{\left(2n_q+1\right)\left((2n_q)!\right)^3} f^{(2n_q)}\left(\xi_\epsilon\right), -1 < \xi_\epsilon < 1. \tag{17}$$

Additionally, the weights of this quadrature rule can be determined by

$$w_i = \frac{2\left(1-x_i^2\right)}{\left(n_q+1\right)^2\left[P_{n_q+1}\left(x_i\right)\right]^2} \tag{18}$$

where x_i are the zeros of the n_q-th Legendre polynomial $P_{n_q}(x)$ and $P_{n_q+1}(x_i)$ is the n_q+1-th Legendre polynomial evaluated at $x = x_i$ with $i = 1 \ldots n_q$.

6. Analytical integrals with respect to r'

The solution for the analytical integration with respect to r' of the integrals associated with the vector potential and the magnetic field intensity in both axial and radial directions are presented in this section. As stated in Section 5, the strategy to be used to solve the integrals associated with the magnetic field of the current carrying disk is the method called *1D Analytical – 1D Numerical*. The analytical expressions have been simplified to the most compact version. Furthermore, intermediate expressions such as ξ_1, ξ_2, and ξ_3 are evaluated once and reused later.

The expressions presented in this section make use of basic mathematical operations (square root, addition, multiplication, etc.) and elementary functions such as the natural logarithm and cosine, ensuring a fast numerical evaluation.

6.1. Magnetic vector potential

According to Section 2.1, the magnetic vector potential due to a current carrying disk with a linear variation of the current density is given by Eq. (5). It can be shown that the magnetic vector potential A_ϕ can be expressed as follows:

$$A_\phi = k_{A1}K_1 + k_{A2}K_2 \tag{19}$$

where k_{A1} and k_{A2} depend solely on the dimensions of the disk and the coordinates of the evaluation point, and K_1 and K_2 are the current densities at the inner and outer radii of the disk respectively. As a result, starting from Eq. (5) and integrating with respect to r' and rearranging, the following expressions for k_{A1} and k_{A2} are obtained

$$k_{A1} = \frac{\mu_0}{2\pi}\int_0^\pi \left(s_a\Big|_{r_i=r_2}\Big|_{r'=r_1}^{r'=r_2} \right) \mathrm{d}\phi' \tag{20}$$

$$k_{A2} = -\frac{\mu_0}{2\pi}\int_0^\pi \left(s_a\Big|_{r_i=r_1}\Big|_{r'=r_1}^{r'=r_2} \right) \mathrm{d}\phi' \tag{21}$$

where

$$s_a = \frac{1}{4\left(r_1 - r_2\right)}\cos\left(\phi'\right)\zeta_1 \tag{22}$$

$$\zeta_1 = \xi_4 + \xi_5\cos\left(\phi'\right) + \xi_6\cos\left(2\phi'\right) \tag{23}$$

$$\xi_1 = \sqrt{r^2 + r'^2 + \left(z - z'\right)^2 - 2rr'\cos\left(\phi'\right)} \tag{24}$$

$$\xi_2 = -r^2 - 2\left(z - z'\right)^2 + r^2\cos\left(2\phi'\right) \tag{25}$$

$$\xi_3 = \ln\left(r' - r\cos\left(\phi'\right) + \xi_1\right) \tag{26}$$

$$\xi_4 = -4r_i\xi_1 + 2r'\xi_1 + \left(r^2 - 2\left(z - z'\right)^2\right)\xi_3 \tag{27}$$

$$\xi_5 = r\left(6\xi_1 - 4r_i\xi_3\right) \tag{28}$$

$$\xi_6 = 3r^2\xi_3 \tag{29}$$

The definite integrals in the expressions of k_{A1} and k_{A2} are to be solved numerically as it will be shown in Section 8.

6.2. Magnetic field intensity in radial direction

Similarly to the case of the vector potential, the proposed corresponding expression for the magnetic field intensity in the radial direction is:

$$H_r = k_{Hr1}K_1 + k_{Hr2}K_2 \tag{30}$$

Performing the innermost partial derivative in Eq. (10), integrating with respect to r' and rearranging, the following expressions for k_{Hr1} and k_{Hr2} can be found

$$k_{Hr1} = -\frac{1}{2\pi}\int_0^{\pi}\left(s_r\Big|_{r_i=r_2}\Big|_{r'=r_1}^{r'=r_2}\right)\mathrm{d}\phi' \tag{31}$$

$$k_{Hr2} = \frac{1}{2\pi}\int_0^{\pi}\left(s_r\Big|_{r_i=r_1}\Big|_{r'=r_1}^{r'=r_2}\right)\mathrm{d}\phi' \tag{32}$$

where

$$s_r = -\frac{\left(z - z'\right)\cos\left(\phi'\right)}{\left(r_1 - r_2\right)\xi_1\xi_2}\zeta_2 \tag{33}$$

$$\zeta_2 = \xi_7 + \xi_8\cos\left(\phi'\right) + \xi_9\cos\left(2\phi'\right) \tag{34}$$

$$\xi_7 = -r^2\left(2r_i + \xi_1\xi_3\right) - 2\left(z - z'\right)^2\left(r_i - r' + \xi_1\xi_3\right) \tag{35}$$

$$\xi_8 = 2r\left(r^2 + r_ir' + \left(z - z'\right)^2\right) \tag{36}$$

$$\xi_9 = r^2\left(-2r' + \xi_1\xi_3\right) \tag{37}$$

The definite integrals in the expressions of k_{Hr1} and k_{Hr2} are solved numerically as shown in Section 8.

6.3. Field intensity in axial direction

Similarly to the case of the magnetic vector potential and the magnetic field intensity in the radial direction, the following expression is proposed:

$$H_z = k_{Hz1}K_1 + k_{Hz2}K_2 \tag{38}$$

Performing the innermost partial derivative of Eq. (13), integrating with respect to r' and rearranging, the following expressions for k_{Hz1} and k_{Hz2} are obtained

$$k_{Hz1} = \frac{1}{2\pi r}\int_0^{\pi}\left(s_z\Big|_{r_i=r_2}\Big|_{r'=r_1}^{r'=r_2}\right)\mathrm{d}\phi' \tag{39}$$

$$k_{Hz2} = -\frac{1}{2\pi r}\int_0^{\pi}\left(s_z\Big|_{r_i=r_1}\Big|_{r'=r_1}^{r'=r_2}\right)\mathrm{d}\phi' \tag{40}$$

where

$$s_z = \frac{1}{4\left(r_1-r_2\right)\xi_1\xi_2}\cos\left(\phi'\right)\zeta_3 \tag{41}$$

$$\zeta_3 = \xi_{10}+\xi_{11}\cos\left(\phi'\right)+\xi_{12}\cos\left(2\phi'\right)+\xi_{13}\cos\left(3\phi'\right)-\xi_{14}\cos\left(4\phi'\right) \tag{42}$$

$$\begin{aligned}\xi_{10} = {} & 4r^4r_i+2\xi_1\xi_2\left(-2r_i\xi_1+r'\xi_1-\left(z-z'\right)^2\xi_3\right)\\ & +r^2\left(4\left(r_i+r'\right)\left(z-z'\right)^2+3\xi_1\xi_2\xi_3\right)\end{aligned} \tag{43}$$

$$\xi_{11} = -4r\left(r^2+r_ir'+\left(z-z'\right)^2\right)\cdot\left(r^2+2\left(z-z'\right)^2\right)+2r\left(5{\xi_1}^2\xi_2-4r_i\xi_1\xi_2\xi_3\right) \tag{44}$$

$$\xi_{12} = r^2\left(4r^2\left(-r_i+r'\right)-4\left(r_i-3r'\right)\left(z-z'\right)^2+9\xi_1\xi_2\xi_3\right) \tag{45}$$

$$\xi_{13} = 4r^3\left(r^2+r_ir'+\left(z-z'\right)^2\right) \tag{46}$$

$$\xi_{14} = 4r^4r' \tag{47}$$

Similarly to the radial field magnitudes, the integrals defined in Eqs (39) and (40) are solved numerically as shown in Section 8.

7. Analysis of singularities

In this section the field expressions where the arguments are undetermined or tend to infinity will be analyzed. This points are called points of singularity or simply singularities. For simplicity's sake, the analysis will be performed only on the magnetic vector potential expressions. The corresponding analysis on the radial and axial magnetic field leads to similar results to those presented in this section.

Consider again the magnetic vector potential according to Eq. (5). The assumption in this case is that $z = z'$ and $r = r_1$, so that the evaluation point is precisely located at the inner radius of the disk. Defining the inner (indefinite) integral with respect to r' of Eq. (5) as follows,

$$S = \int f_A\left(\phi', r'\right)\mathrm{d}r' \tag{48}$$

the magnetic vector potential is given by

$$A_\phi = \frac{\mu_0}{2\pi}\int_0^{\pi} S\Big|_{r'=r_1}^{r'=r_2}\mathrm{d}\phi' = \frac{\mu_0}{2\pi}\left(\int_0^{\pi} S\Big|_{r'=r_2}\mathrm{d}\phi' - \int_0^{\pi} S\Big|_{r'=r_1}\mathrm{d}\phi'\right) \tag{49}$$

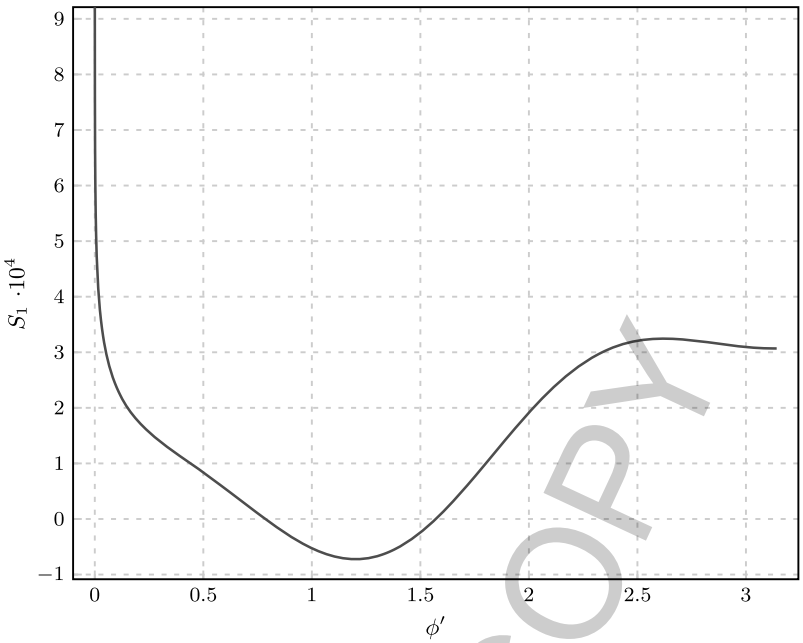

Fig. 2. Behavior of S_1 as a function of ϕ'.

The integral $\int_0^{\pi} S|_{r'=r_2} \mathrm{d}\phi'$ is free of singularities; therefore, the attention is to be focused on the second integral. The integration and evaluation of S for $r' = r_1$ yields

$$\begin{aligned} S_1 = S\Big|_{r'=r_1} &= \frac{1}{4\left(r_1 - r_2\right)} \cos\left(\phi'\right) \\ &\cdot \Bigg(2r_1 \sqrt{2 - 2\cos\left(\phi'\right)} \left(\left(K_1 + K_2\right) r_1 - 2K_1 r_2 + 3\left(K_1 - K_2\right) r_1 \cos\left(\phi'\right) \right) \\ &+ r_1 \left(4\left(K_2 r_1 - K_1 r_2\right) \cos\left(\phi'\right) + \left(K_1 - K_2\right) r_1 \left(1 + 3\cos\left(2\phi'\right)\right) \right) \\ &\cdot \ln\left(r_1 \left(1 + \sqrt{2 - 2\cos\left(\phi'\right)} - \cos\left(\phi'\right) \right) \right) \Bigg) \end{aligned} \tag{50}$$

It can be seen that S_1 is singular at $\phi' = 0$. To investigate the behavior of Eq. (7) for varying ϕ', a scenario is proposed with the following disk data:

$$\begin{aligned} K_1 &= -10,000 \text{ A/m} \\ K_2 &= 10,000 \text{ A/m} \\ z' &= 3 \text{ m} \\ r_1 &= 1 \text{ m} \\ r_2 &= 2 \text{ m} \end{aligned}$$

Figure 2 depicts S_1 in the range $\phi' = (0, \pi]$. An asymptotic behavior of the function at $\phi' = 0$ can be easily seen.

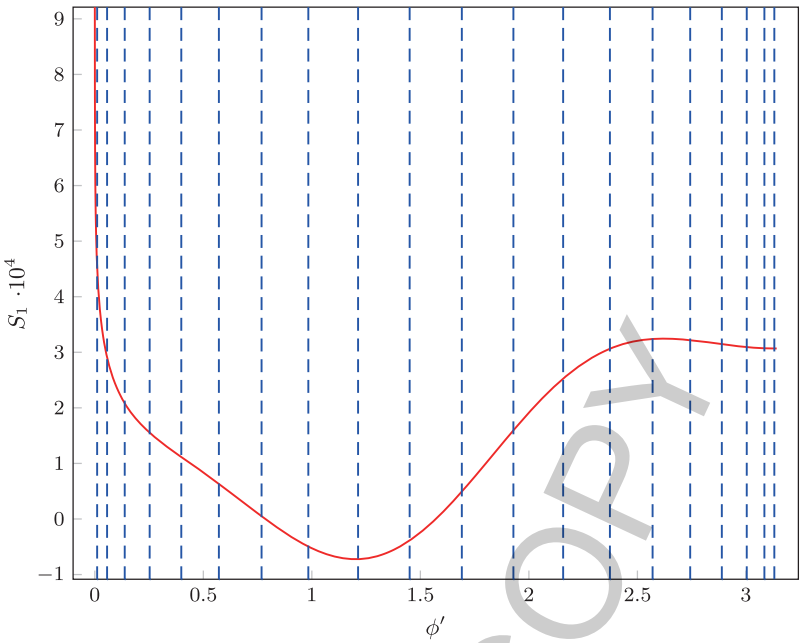

Fig. 3. Plot of S_1 including 20 nodes of the Gauss-Legendre quadrature as dotted lines.

As stated in Section 5, the Gauss-Legendre quadrature with a direct integration scheme has been selected for the integration task. Figure 3 shows S_1 along with the coordinates of 20 Gauss-Legendre quadrature nodes, which have now been indicated using vertical dotted lines. It can be seen that the distance between nodes becomes smaller near to the limits of integration as required. To assess the behavior of the quadrature near to the singularity, Fig. 4 depicts the results of Fig. 3 again, but this time in the range $\phi' = (0, 1/2]$. It has been found that the function variation within the range of these first 5 nodes is very important, which suggests that the number of nodes must be increased to improve the resolution of the quadrature near the singularity.

Figure 5 shows the function S_1 in the range $\phi' = (0, 1/2]$, but using 100 Gauss-Legendre quadrature nodes. As shown, the discretization level near the singularity is quite consistent with the variation of the function, which increases the accuracy of the calculation.

The numeric values found by evaluating S_1 using 20 nodes, 100 nodes and by means numerical adaptive integration using Wolfram Mathematica® are given as follows:

$$\int_0^{\pi} S_1 \mathrm{d}\phi' \approx 44,553.9129 \rightarrow \text{ 20 nodes, Gauss-Legendre}$$

$$\int_0^{\pi} S_1 \mathrm{d}\phi' \approx 44,599.1700 \rightarrow \text{ 100 nodes, Gauss-Legendre}$$

$$\int_0^{\pi} S_1 \mathrm{d}\phi' \approx 44,601.1339 \rightarrow \text{ Adaptive Mathematica}$$

It can be seen that although the solutions using 20 and 100 nodes are very close to the one found by Mathematica (which is taken as a reference), the error term E_n is 1.9639 using 100 nodes and 47.2210 using 20 nodes. Furthermore, the relative error of the calculated value using 100 nodes related to the reference value is less than 0.005 %.

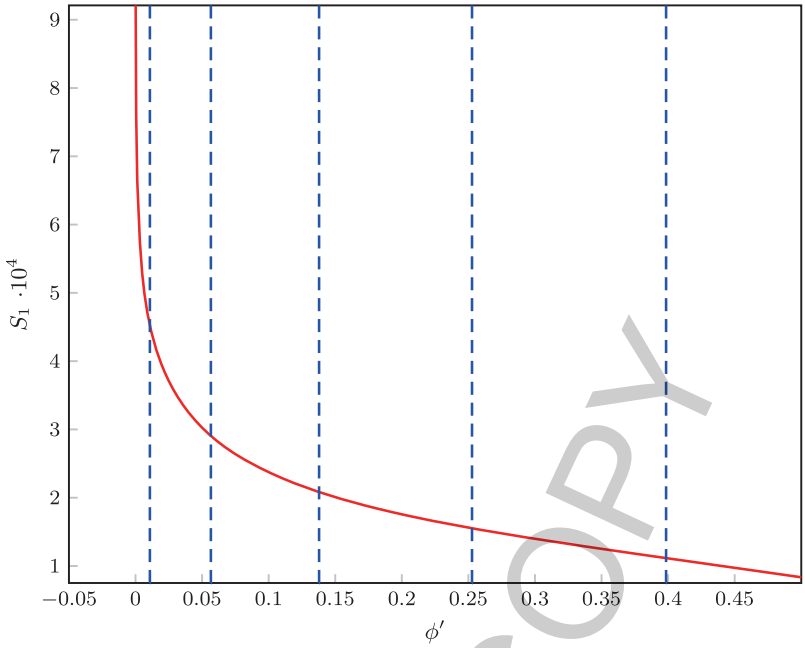

Fig. 4. Plot of S_1 including 20 nodes of the Gauss-Legendre quadrature as dotted lines.

Two important conclusions can be drawn from the performed analysis of singularities. The first one is that the integrands have singularities at one of the limits of integration, and the second one is that the Gauss-Legendre quadrature naturally avoids the singularity and makes possible the correct estimation of the integral in this situation.

8. Numerical integration with respect to ϕ'

This section briefly introduces the methodology used to determine the numerical solution of the integrals associated with the disk (Eqs (20), (21), (31), (32), (39) and (40)). A significant amount of sources (disks) and evaluation points (n_s and n_f respectively) will be considered. The general expression of all integrals to be solved can be written as

$$S_\phi = \int_0^\pi f\left(\phi', r_1, r_2, z', r, z\right) \mathrm{d}\phi' \tag{51}$$

In the context of this article, the term interaction is used to describe the influence produced by each source at each evaluation point. For example, if there are 100 disks and 100 evaluation points, it would be a total of $10,000$ interactions. Consequently, the task is to solve $(n_s \cdot n_f)$ integrals like S_ϕ. Because the number of interactions can be very large, the calculations must be as efficient as possible.

The traditional solution for this problem would be to calculate each integral by solving the summation in Eq. (15) by means of two nested loops. However, this method is not efficient because it is an entirely serial process and additionally the same nodes and weights of the quadrature have to be read and applied $(n_s \cdot n_f)$ times, which takes a lot of computation time unnecessarily. Furthermore, there is no savings in the calculation since the products and sums are calculated one by one.

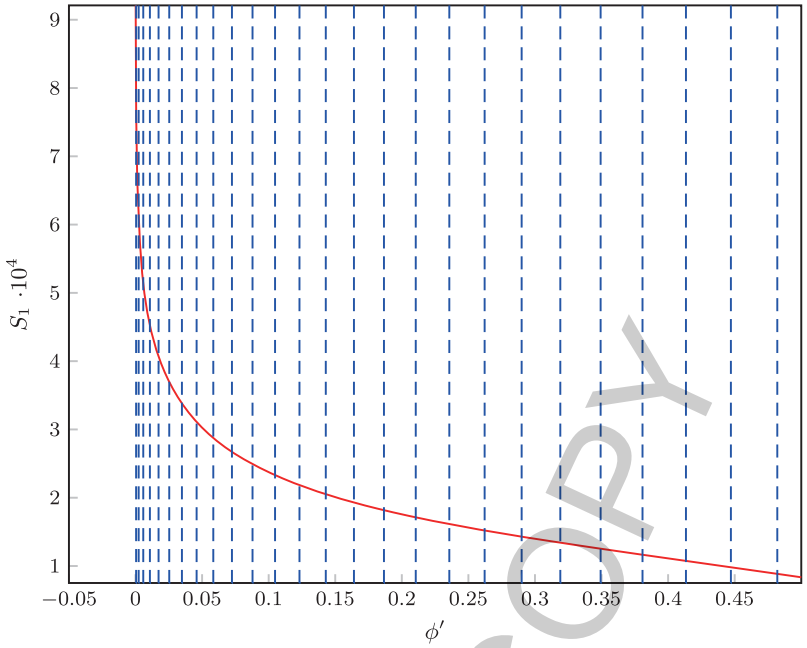

Fig. 5. Plot of S_1 including 100 nodes of the Gauss-Legendre quadrature as dotted lines.

Assume that all integrals are evaluated using a fixed amount of n_q nodes, which are arranged in a column vector with n_q rows denoted as $\mathbf{x}^{[n_q \times 1]}$. Similarly, a weight vector $\mathbf{w}^{[n_q \times 1]}$ is defined. According to the transformation presented in Section 3, the coordinates of the nodes are given by $\boldsymbol{\phi}' = c \cdot \mathbf{x} + d$.

A matrix of $(n_s \cdot n_f)$ rows and n_q columns denoted as $\mathbf{F}^{[n_s \cdot n_f \times n_q]}$ is defined in order to properly keep the values of the function $f(\phi', r_1, r_2, z', r, z)$ evaluated in all possible combinations of sources, evaluation points and nodes. The solution of all the integrals can thus be found in one step using the following matrix product

$$\mathbf{s} = c \cdot \mathbf{F} \cdot \mathbf{w} \tag{52}$$

where $\mathbf{s}$ is a column vector containing the solutions of the $(n_s \cdot n_f)$ integrals.

Since this is a matrix process, the iterative calculation of the summation of Eq. (15) is possible at a lower computational complexity compared with the traditional term by term calculation. This is achieved through the use of libraries such as LAPACK or specialized programs for matrix calculation such as Matlab®, which in addition to providing specialized techniques of matrix algebra, also provide support for parallel processing on multiple cores. See reference [14] for a detailed treatment of the computational complexity of matrix product.

8.1. Selection of the number of nodes

It can be seen from Fig. 1 that except for the condition $0 < r_1 < r_2$, the variables describing the problem (r_1, r_2, z', K_1, K_2, r and z) can vary in the arbitrary range $(-\infty, \infty)$. This makes the error analysis a challenging task if the results of the methodology are supposed to cover all possible cases, which are obviously infinite.

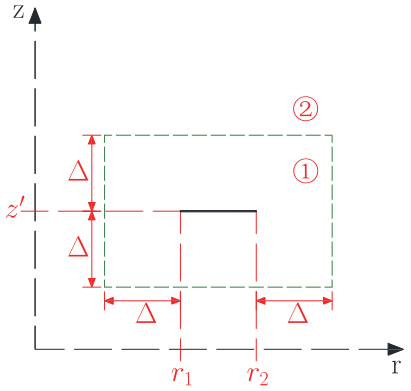

Fig. 6. Regions for the selection of the number of nodes.

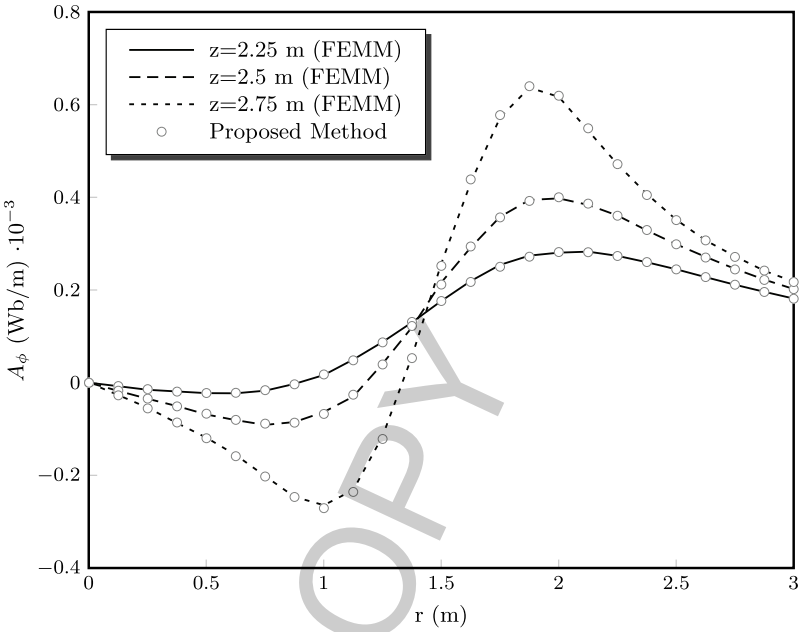

Fig. 7. 2D plot of the magnetic vector potential of the disk.

So far, it was considered that the numerical integration involves a number of nodes n_q, however, nothing has been said about the practical value of this quantity. For the error analysis, the ranges considered for the variables are limited to orders of magnitude that are typical of engineering applications, considering geometric dimensions from a few millimeters to a few tens of meters.

A systematic analysis of the error within these ranges has been performed and the following general conclusions have been found:

- The maximum error values are at singularity points and close to the disk surface.
- The farther the evaluation point (r, z) is from the source, the lower the error.
- The values of current densities K_1 and K_2 does not significantly affect the behavior of the error.

Clearly, assuming an unlimited computational resource (which is not the real case), the use of an extremely large number of nodes could be considered, so that the error could be bounded at the points nearest to the disk surface. The practical problem of applying this type of strategy is that fewer nodes are needed at far evaluation points to achieve the desired accuracy. The use of a fixed number of nodes for these far points would therefore result in a large amount of unnecessary calculations, so that it is not convenient to use a fixed number of nodes derived from the most demanding error criterion. A practical approach has been developed which proved to be reliable and accurate, which is discussed below.

For each disk, the space is divided into two regions ① and ② as shown in Fig. 6. In this way, the field points that fall within the ring with rectangular cross-section denoted by ① are to be evaluated with an amount of n_{q1} nodes. The remaining field points that fall into region ② will be evaluated using n_{q2} nodes. It has been additionally assumed that the points that fall at the boundary between both regions are to be evaluated with n_{q2} nodes.

It has been established that the criterion for the size of the region ① is $\Delta = |r_2 - r_1|$. In case that $\Delta > r_1$, then $\Delta := r_1$. Additionally, it was found from the numerical evaluation of hundreds of different random cases, that using $n_{q1} = 100$ and $n_{q2} = 20$ an appropriate engineering accuracy can be achieved.

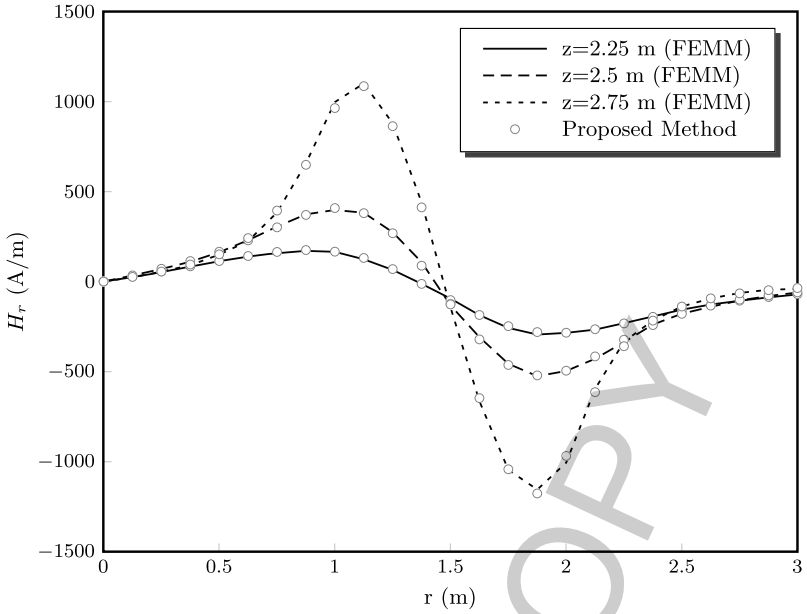

Fig. 8. 2D representation of the magnetic field intensity of the disk in the radial direction.

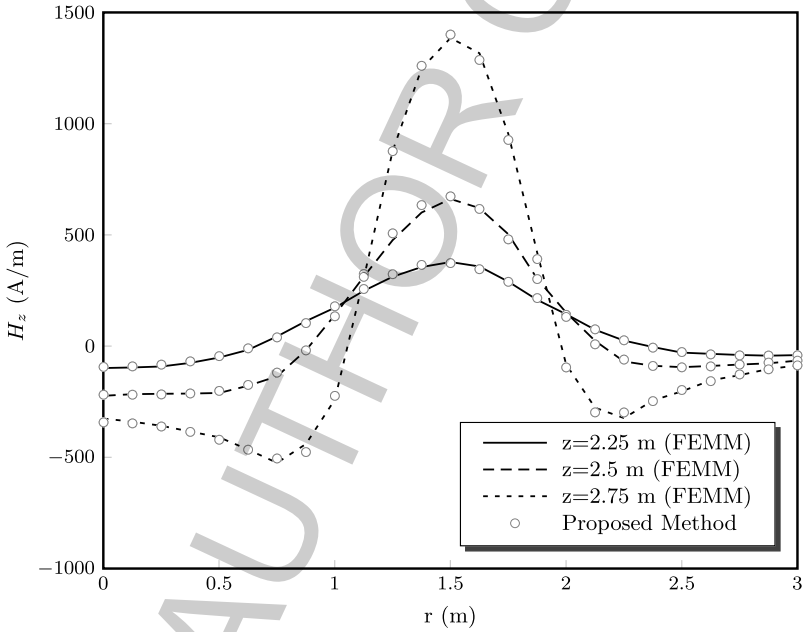

Fig. 9. 2D representation of the magnetic field intensity of the disk in the axial direction.

The analysis performed in this section has been called *off-line analysis* of the error, because the most critical cases have been analyzed off-line and a predefined appropriate amount of nodes have been chosen for each region. Additionally, the nodes and weights have been precomputed through specialized routines so that they are directly available when needed, avoiding its calculation during the integration process.

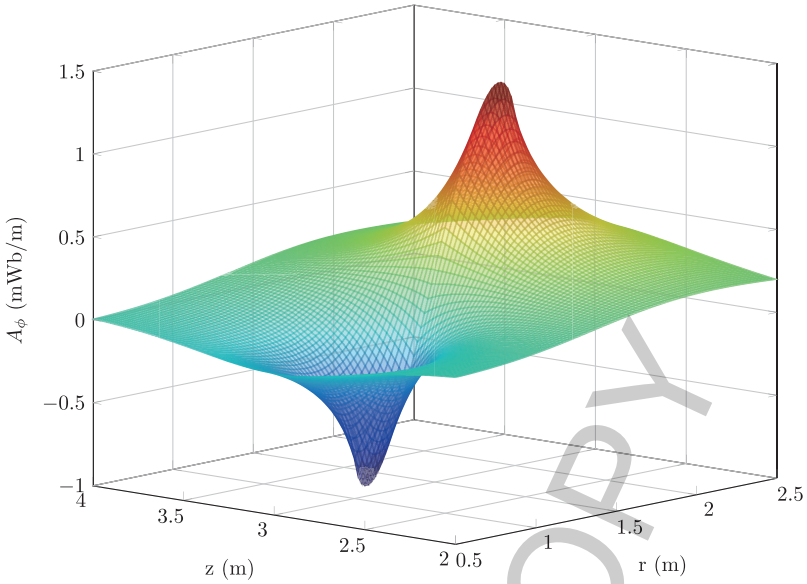

Fig. 10. Magnetic vector potential of the disk.

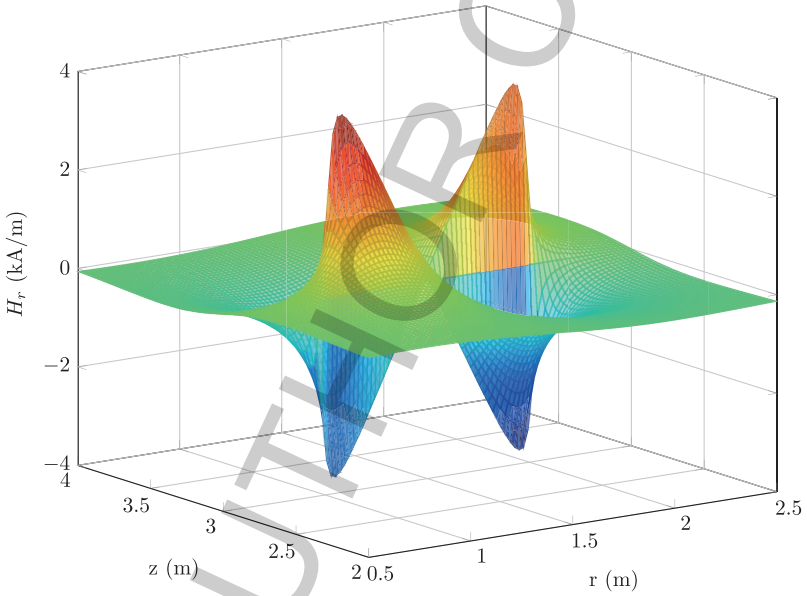

Fig. 11. Magnetic field Intensity of the disk in the radial direction.

9. Validation using the finite element method

In order to verify the validity of the methodology presented in this work, the example case presented in Section 7 ($K_1 = -10,000$ A/m, $K_2 = 10,000$ A/m, $z' = 3$ m, $r_1 = 1$ m, $r_2 = 2$ m) is calculated using the proposed method, and the results compared with those of the Finite Element Method (FEM). The FEM software used in this case was the program Finite Element Method Magnetic (FEMM) [15].

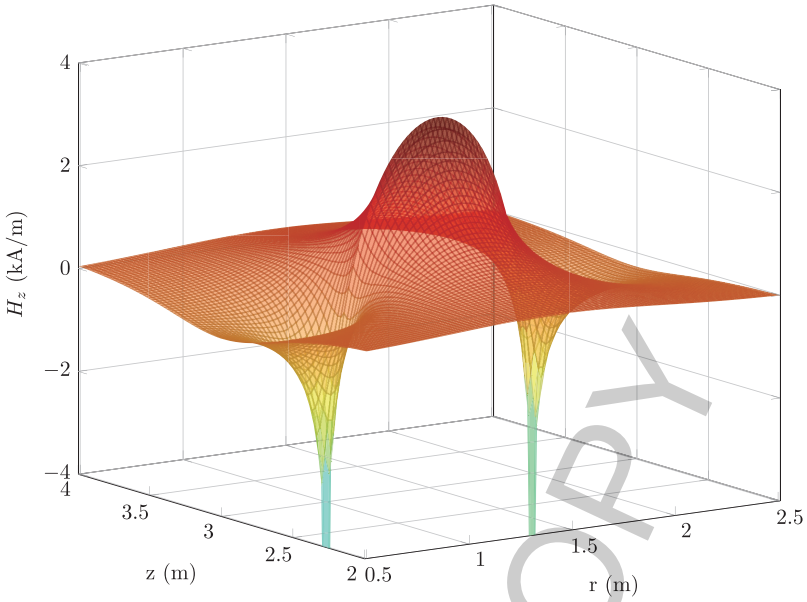

Fig. 12. Magnetic field Intensity of the disk in the axial direction.

In order to model the linear variation of current density in the disk using FEM, a set of 500 subdisks having 1 mm thick have been used, each of them having a current value that satisfies the current density distribution of Eq. (2). The outer boundary of the problem has been modeled by a sphere of radius 6 m with mixed type boundary condition to emulate an open domain. The mesh used was the default mesh generated by the program.

Figures 7–9 show 2D plots of the field distribution due to the disk used as an example for the planes $z = 2.25$, $z = 2.5$ and $z = 2.75$. The magnetic field calculations performed by FEMM has been plotted using dashed and solid lines, while circle labels indicate the values calculated using the methodology presented in this work. As it can be seen, both solutions virtually overlap in the three figures, confirming the validity of the model presented. Additionally, Figs 10–12 show the 3D distribution of the magnetic vector potential and the magnetic field intensity in radial and axial directions of the disk respectively.

10. Conclusions

This paper presents a new methodology to determine the magnetic field produced by a geometric disk-shaped configuration considering the linear variation of the sheet current density. The methodology proposed in this work has evidenced as fast, accurate and free of singularities for the purposes of engineering applications considering multiple sources and evaluation points.

The Gauss-Legendre quadrature has proven to be a quite adequate tool for solving the proposed problem because naturally avoids the singularities and concentrates more nodes in a convenient way near to them.

In the proposed methodology, the most computationally expensive tasks have been performed off-line, such as the error analysis and determination of the weights and nodes. Additionally, they have been reused ($n_f \cdot n_s$) times, which significantly reduces computing time with respect to adaptive integration methods. The computationally most expensive task of the proposed methodology is the evaluation of the

function for all ($n_q \cdot n_f \cdot n_s$) combinations. However, the analytical formulas presented are quite compact and are expressed through elementary functions of very quick evaluation.

To summarize, it can be concluded that the three concepts that make successful the proposed methodology are the vectorization, the reuse of calculation results and the off-line analysis of the error.

Acknowledgments

This work has been supported by the German Academic Interchange Service (DAAD) as part of a scholarship for doctoral studies in Electrical Engineering in the Universidad Nacional de San Juan, located in San Juan, Argentina. Acknowledgments are also made to Siemens A.G. in Nuremberg-Germany and Siemens Andina Transformers Bogotá-Colombia, which have provided the motivation for this research.

References

[1] S.V. Kulkarni and A. Bakshi, Analysis of winding disk in transformer under action of axial electromagnetic forces by Green's function approach, *International Journal of Applied Electromagnetics & Mechanics* **34** (2010), 237–247.
[2] I. Doležel, P. Karban and P. Šolín, Integral methods in low-frequency electromagnetics: Wiley-Interscience, 2009.
[3] S. Babic and C. Akyel, New closed-form expressions for calculation of magnetic field of thin ring conductors with current-carrying in azimuthal and radial directions, *Microwave Conference Proceedings, APMC '97, Asia-Pacific* **1** (1997), 201–204.
[4] S. Babic, C. Akyel, S.J. Salon and S. Kincic, New expressions for calculating the magnetic field created by radial current in massive disks, *Magnetics, IEEE Transactions on* **38** (2002), 497–500.
[5] B. Azzerboni and E. Cardelli, Magnetic field evaluation for disk conductors, *Magnetics, IEEE Transactions on* **29** (1993), 2419–2421.
[6] B. Azzerboni, G. Saraceno and E. Cardelli, Three-dimensional calculation of the magnetic field created by current-carrying massive disks, *Magnetics, IEEE Transactions on* **34** (1998), 2601–2604.
[7] H. Knoepfel, Magnetic fields, a comprehensive theoretical treatise for practical use, John Wiley & Sons, Inc., New York, 2000.
[8] P. Kythe and M. Schäferkotter, Handbook of computational methods for integration, Chapman & Hall/CRC Press, 2005.
[9] W. Smythe, Static and dynamic electricity, McGraw-Hill , New York, 1950.
[10] M. Abramowitz and I. Stegun, Handbook of mathematical functions with formulas graphs amd mathematical tables, Dover Publications Inc., New York, 1970.
[11] G. Díaz, E. Mombello and V. Stephan, Magnetic vector potential and magnetic field intensity due to a finite current carrying cylinder considering a variable current density along its axial dimension, *International Journal of Applied Electromagnetics & Mechanics* **40**(2) (2012).
[12] C. Hastings, Approximations for digital computers, Princeton Uneversity Press, New Jersey, 1955.
[13] S. Zhang and J. Jin, Computation of special functions, John Wiley & Sons, Inc., New York, 1996.
[14] S. Robinson, Toward an optimal algorithm for matrix multiplication, *SIAM News* **38**(9) (2005).
[15] D.C. Meeker, Finite element method magnetics, Version 4.2 (x64) (01Oct2011 Build), http://www.femm.info.